Journal of Electronics, Electromedical Engineering, and Medical Informatics
Multidisciplinary: Rapid Review: Open Access Journal Vol. 7, No. 1, January 2025, pp: 47-55; eISSN: 2656-8632

RESEARCH ARTICLE OPEN ACCESS

Manuscript received July 25, 2024; revised August 10, 2024; accepted August 20, 2024; date of publication November 11, 2024
Digital Object Identifier (**DOI**): https://doi.org/10.35882/jeeemi.v7i1.525

Copyright © 2024 by the authors. This work is an open-access article and licensed under a Creative Commons Attribution-ShareAlike 4.0 International License (CC BY-SA 4.0).

How to cite: G.Naga Chandrika, Rini Chowdhury, Prashant Kumar, Sangamithrai K, Glory E and Saranya M D, " Conjugated Pixel Grouping Scheme for COVID-19 Detection from X-Ray Images Using Adversarial Learning", Journal of Electronics, Electromedical Engineering, and Medical Informatics, vol. 7, no. 1, pp. 47-55, January 2025.

Conjugated Pixel Grouping Scheme for COVID-19 Detection from X-Ray Images Using Adversarial Learning

G.Naga Chandrika[1], Rini Chowdhury[2], Prashant Kumar[2], Sangamithrai K[3], Glory E[4] and Saranya M D[5]

[1] Department of Information Technology, VNR VJIET, Hyderabad, Telangana, India
[2] Department of Information Technology Project Circle BSNL, Saltlake Telephone Exchange, Block DE, Lalkuthi, West Bengal, Kolkata, India
[3] Department of Computer Science and Engineering, Vel Tech Rangarajan Dr. Sagunthala R&D Institute of Science and Technology, Chennai, Tamilnadu, India.
[4] Department of Computer Science, Vels Institute of Science, Technology & Advance Studies Velan Nagar, Pallavaram, Chennai, India
[5] Department of ECE, KPR Institute of Engineering and Technology, Coimbatore, India, India.

Corresponding author: Glory E (e-mail: titu332@gmail.com).

ABSTRACT COVID-19 detection from X-ray images is eased through machine learning and computational intelligent algorithms for precision-focused diagnosis. The infection spread is identified using pixel variations observed at different X-ray regions using conventional image processing techniques. To this extent, this article proposes a Conjugated Pixel Grouping Scheme (CPGS) introduced to improve the precision of COVID-19 detection from X-ray inputs. This scheme addresses the concentric boundary problem due to assorted pixel distribution. The problem using the proposed scheme is addressed using pre-activated adversarial learning. The activation is used to detect conjugation between identified and unidentified pixels along the input distribution. The grouping is performed by adversarial learning that classifies the activated and non-activated distributions. This process is thus sequential for grouping classified conjugations to identify the infected region from non-conjugated distributions. The boundary is marked between the classified and unclassified regions to improve the pre-activation in the consecutive distributions. The proposed scheme improves the detection accuracy and precision by 9.03% and 8.76% respectively and reduces classification error by 10.17% for the maximum number of boundaries.

INDEX TERMS Activation Function, Adversarial Learning, Boundary Detection, COVID Detection, X-Ray

I. INTRODUCTION

COVID-19 can be diagnosed by making use of imaging X-rays since it can reveal the presence in the lungs for an accurate diagnosis [1]. Ground-glass opacities and lung consolidation through images in X-rays may be regarded as specific markers for COVID-19 infection. Such kind of method is non-invasive and very accessible because virtually each health facility has an X-ray machine in place [2]. X-rays help in follow-up tracking of the disease to know the extent of lung involvement, therefore formulating management strategies [3]. The ability has been key during the pandemic as the care management by the patients has to be managed. X-ray imaging for detecting symptoms of COVID-19 can be used for large-scale screening processes, providing big chances for early interventions and significantly improved results. Medical treatment and management become efficient in trying to combat the virus by easily identifying infections in patients and fastens the management process [4, 5].

The use of machine learning (ML) for the detection of COVID-19 in X-ray images enhances diagnostic capabilities through automation and improvement in the analysis of images [6]. Convolutional neural networks (CNN) have been trained on specific features of X-ray images produced as the result of lung damage from COVID-19. These models provide differentiation at a high precision among all respiratory diseases and COVID-19, which is the key to an accurate diagnosis [7]. ML cuts the period that radiologists and healthcare workers will take to analyze the images, thus saving time for quicker decision-making and treatment planning [8]. Algorithms are learning from increasing data, that is enhancing the accuracy of new mutations in viruses and patterns in images. The combination of machine learning with X-ray images accelerates the process of diagnosis and thus makes health care more efficient. Such a combination is especially helpful in health care for high-demand systems during the pandemic of COVID-19 [9, 10]. The contributions of the article are:

1. To perform a background study of different methods related to COVID-19 detection from X-ray images using different machine-learning techniques
2. To propose a novel conjugated pixel groping scheme to avoid the concentric boundary problem that reduces the detection precision of infected regions
3. To validate the proposed scheme's performance using accuracy, precision, classification error, and time metrics
4. To verify the efficiency of the proposed scheme using a comparative analysis alongside MTSS-AAE [18] and SD-GAN [14] methods

The article's organization is as follows: Section 2 presents the related works, describing different proposals from various authors. Section 3 describes the proposed scheme with its derivatives and diagrammatic illustrations. In Section 4, the experimental and comparative analysis results are presented followed by the conclusion, limitations, and future scope in Section 5.

II. RELATED WORKS

Naz et al. [11] designed a centralized and federated learning (FL) based COVID-19 detection using chest X-ray (CXR) images. The FL algorithm is employed here to analyze the CXR dataset and produce relevant features for detection. The model evaluates both global and spatial parameters from the information which decreases the delay ratio of the system. The designed model maximizes the accuracy range of the disease detection process. Li et al. [12] introduced a residual capsule network-based COVID-19 detection. CXR images are used as inputs which provide discriminative features and details for further processes. An extraction technique is used here to extract the prominent features from the dataset. The capsule network detects the exact types of COVID-19 for the disease diagnosis process. The introduced framework increases the classification precision level of the disease.

Li et al. [13] proposed an integrated convolutional neural network (CNN) algorithm and FL-enabled COVID-19 detection method using CXR images. The proposed method detects the exposing source data which are presented in CXR images. The detected data is used as inputs which reduces the energy consumption range of the process. Experimental results show that the proposed method enhances the accuracy and efficiency ratio of the detection system. Kausar et al. [14] developed a style distribution transfer generative adversarial network (SD-GAN) model for COVID-19 detection via X-ray images. It is an automated model which detects the disease according to the features in X-ray images. The unwanted noises that are presented in the images are eliminated to get fine features for the detection process. The developed model improves the accuracy and feasibility range of COVID-19 detection. An improved version of [13] is designed by Thangaraj et al. [15] for automated COVID-19 detection.

The designed method uses a feature fusion approach to fuse the important features from CXR images. A transfer learning (TL) algorithm is also employed here to identify the class of the features. The TL algorithm minimizes the computational cost and latency of the process. The designed method elevates the accuracy level of disease detection. Alshahrni et al. [16] proposed an intelligent deep CNN-based COVID-19 detection model using CXR images. It is a hybrid model which decreases the error rate while classifying the diseases. The proposed model pre-processes the trained values which are gathered via CXR images. When compared with others, the proposed model enlarges the accuracy range of the detection process. George et al. [17] introduced a new homomorphic transformation filter-enabled COVID-19 disease detection approach using CXR images. The introduced approach uses a deep CNN algorithm to extract relevant features from the given images. The filter identifies the effective features that are located on the images and eliminates the unwanted images from the dataset. The introduced approach achieves high accuracy in disease detection and classification processes. Ullah et al. [18] developed a multi-task semi-supervised adversarial autoencoding (MTSS-AAE) model using CXR images for COVID-19 detection. The developed model identifies the discriminative features that produce feature data for the detection process. The AAR module is used here to evaluate the small set of data and to gather relevant values from the datasets. The developed MTSS-AAE model improves the performance and precision level of disease detection. Bhattacharjee et al. [19] proposed a new deep learning (DL) model using CXR images for COVID-19 detection. It is used as an effective classification model which classifies the actual stages of COVID-19. The proposed model produces robust features and parameters that are trained for disease detection. Experimental results show that the proposed model enlarges the accuracy range of the detection systems. Liang et al. [20] introduced a correlation-based multi-scale feature fusion network (CMFuse) for COVID-19 using CXR images. The introduced method uses an AI technique to assist the dataset which is collected from the images. A CNN algorithm is implemented in the method to analyze the spatial and temporal features from collected data. The introduced method increases the specificity, accuracy, and robustness level of the process.

The proposed scheme addresses the concentric boundary problem identified in the uneven pixel distribution of X-ray images for COVID-19 detection. This problem is identified due to different pixel features extracted from different regions with multiple patterns. If the features extracted are non-classified, then the region detection using the individual patterns is less feasible to achieve maximum precision. Therefore, to avoid this problem, a conjugated pixel grouping scheme is proposed. This scheme avoids the boundary error problem using pixel distribution classification using pre and post-activation functions.

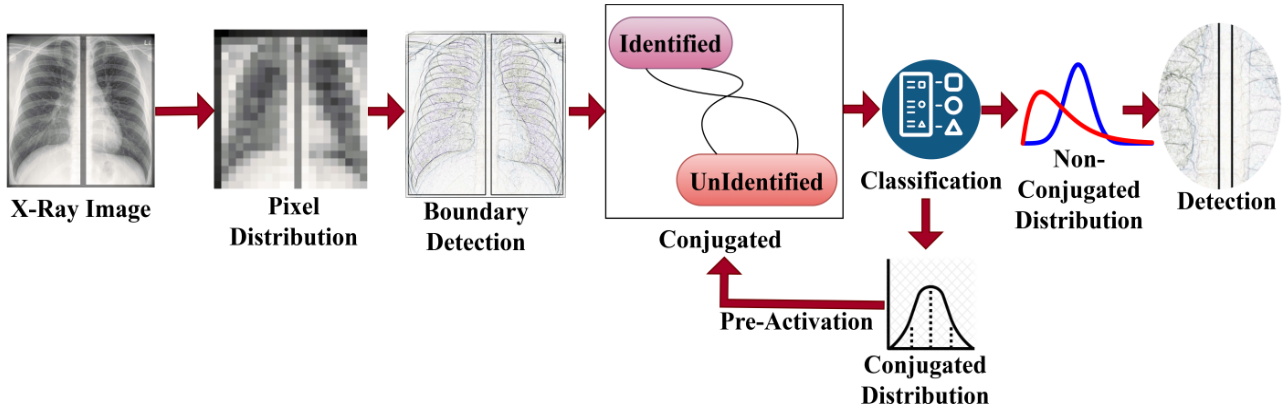

FIGURE 1. Schematic Illustration of the Proposed CPG Scheme

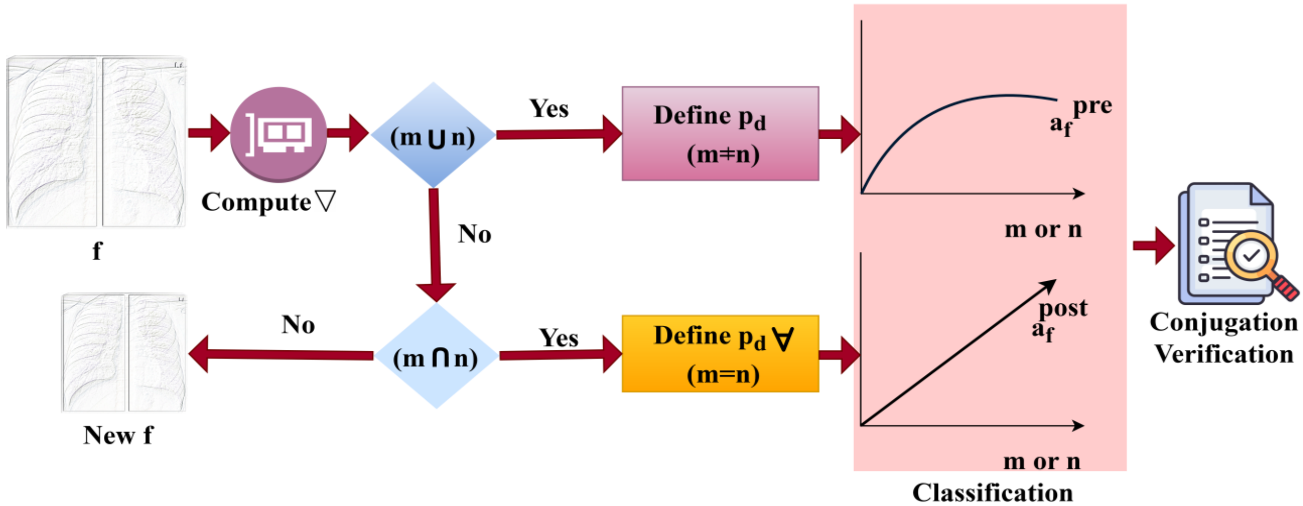

FIGURE 2. Classification for Conjugation

III. PROPOSED CONJUGATED PIXEL GROUPING SCHEME

The proposed scheme is introduced to reduce the concentric boundary problem observed in processing X-ray images for COVID-19 detection. The random pixel distribution observed in X-ray images results in concentric and overlapping features. Such features reduce the precision if the image size increases. This proposed scheme reduces the aforementioned issue using pre-activated adversarial learning. A schematic illustration of the proposed scheme is presented in FIGURE 1. The X-ray image input is examined for its pixel distribution followed by the boundary detection. This boundary detected is temporal from which pixel (individual) identification and un-identification are classified [21]. The conjugation (explained later) factor decides the activation and detection using modified boundary positions (FIGURE 1). Therefore, the process is explained from the pre-activated to the learning process described below.

A. Pixel Distribution Estimation

Let $(m \times n)$ denote the input X-ray image input characterized by $(m \times n)$ pixels denoting the maximum size of the image. If f is the set of features in $(m \times n)$, then pixel distribution (p_d) is defined as in Eq.(1).

$$p_d = \begin{Bmatrix} [\sum f * m] + [(\sum f - 1) * n] - [\sum f - (m \cap n)], \forall m \neq n \\ (\sum f * m) \| (\sum f * n) - [(\sum f - 1)], \forall m = n \end{Bmatrix} \quad (1)$$

In Eq.(1), the formal distribution is computed for $(m \neq n)$ and $(m = n)$ cases. This implies the random and similar feature (f) distribution that is extractable. In this case, if pre-activation is initiated, then it prefers both the differentiation cases that are refined in the consecutive learning iterations [22]. The difference in distribution for boundary detection is estimated along the p_d. In this case, if the difference is maximum, then a boundary is detected else the p_d is computed for new f. This difference (∇) for boundary detection is computed in Eq.(2).

B. Pre-Activation function

The pre-activation function defines the conjugation demand for multiple ∇ classifications. In the pre-activation process,

TABLE 1
Sample Input and Findings

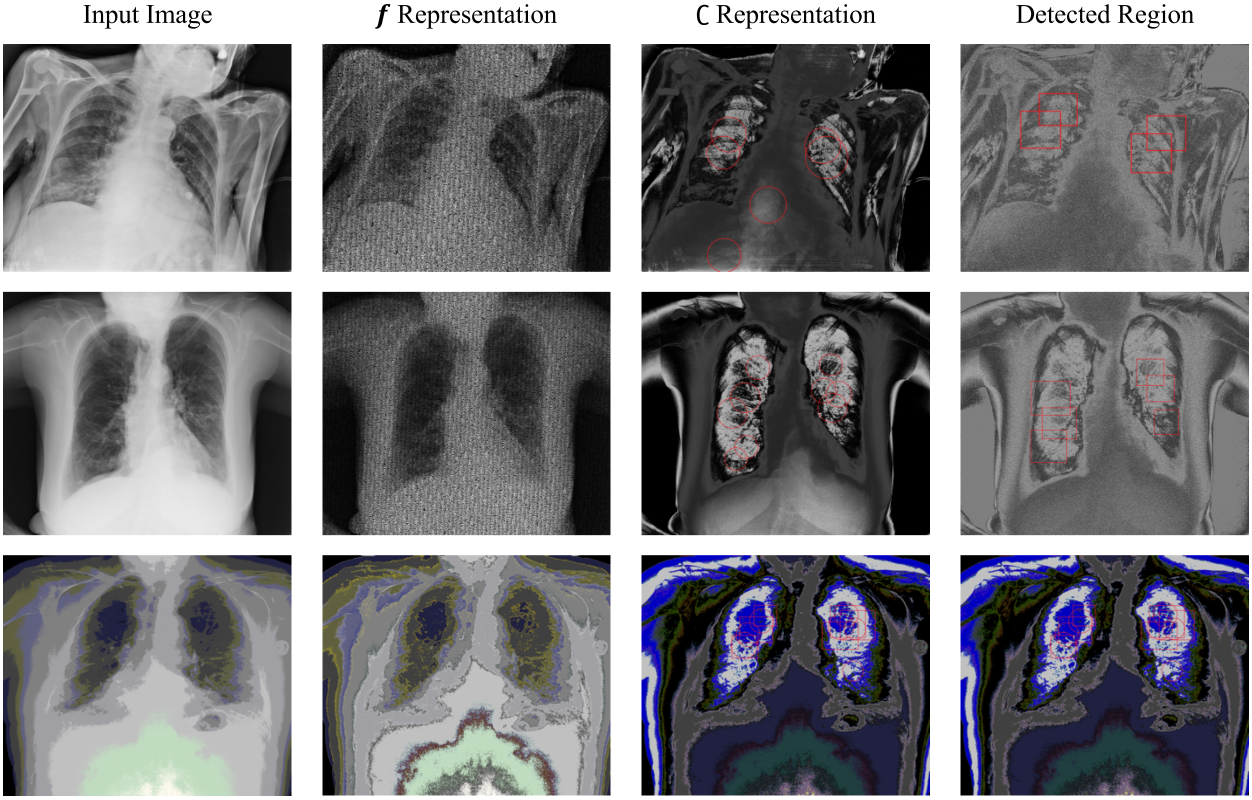

the identified and unidentified f from ∇ are used to validate new boundaries for COVID-19 infected region detection. Therefore, the activation function (a_f) is defined as in Eq.(3).for pre and post-categorization of ∇ its minimum and maximum outputs.

$$a_f^{pre} = \begin{Bmatrix} fm^2 + fn - \nabla \| fn^2 + fm - \nabla, \forall(m \cup n) \\ (fm - \nabla) \| (fm - \nabla) \forall(m \cap n) \end{Bmatrix}$$
$$a_f^{post} = \begin{Bmatrix} fm + fn + \left(p_d * \frac{1}{\nabla}\right) - \sum(m \cap n) \\ fm + \left(p_d * \frac{1}{\nabla}\right) - \sum(m \cup n) \end{Bmatrix} \quad (3)$$

The above activation function defines the need for conjugation as concluded by the $(m \cup n)$ and $(m \cap n)$ differences. However, the first is used for single variant boundaries detected whereas the latter is used for duo variants ∇. Therefore, the activation function defined for conjugation classification is presented in FIGURE 2.

$$\nabla = \begin{Bmatrix} [f - (m \cap n)] \forall m \neq n \\ (f - m) \| (f - n) \forall (m = n) \\ such\ that\ maximum = (m \cup n)\ and\ minimum = (m \cap n) \end{Bmatrix} \quad (2)$$

This difference between the maximum and minimum feature p_d distinguishes two boundaries. If there are any f present between $\nabla = maximum$ and $\nabla = minimum$ then pre-activation is required. In contrast, the duo alone halts the pre-activation where conjugation assessments are performed. The classification is presented in FIGURE 2 based on the extracted f and ∇. If the ∇ is large (maximum), then $p_d \forall (m \neq n)$ under $(fm^2 + fn - \nabla)$ is the classification. Else the p_d for m (or) n is the minimal output for $a_{f_{pre}}^{post}$ and the successive iterations pursue a_f^{post} from which its reduction takes place. Therefore, other than duo boundary detection, the non-zero classification relies on non-conjugated p_d from a_f^{pre}, then a_f^{post} is used and thereby detection is performed. Thus, the next process is the conjugation of p_d that is described below.

C. Conjugation Process of p_d

The term conjugation refers to the mixed p_d and f existence in any $(m \times n)$ irrespective of their evenness. Therefore, the conjugation (C) defines the existence of $(m \times n) \forall (m \cap n)$ and $(m \cup n)$ under the same f; the boundary is different. The ∇ classifies the minimum/maximum difference between multiple p_d factor [23]. Therefore, to consolidate the distribution adversarial learning is used in this scheme. First, C is defined as in Eq.(4).

$$C = \begin{Bmatrix} \frac{1}{1+\nabla^{1/n}} + \frac{n+\nabla^{1/n}}{\nabla^n - \nabla^{1/n}} \forall (m \cup n) \Rightarrow maximum \\ \frac{1}{\nabla} * \left(\frac{\nabla^n - \nabla^{\frac{1}{n}}}{\nabla^n + \nabla^{\frac{1}{n}}}\right) \forall (m \cap n) \Rightarrow minimum \end{Bmatrix} \quad (4)$$

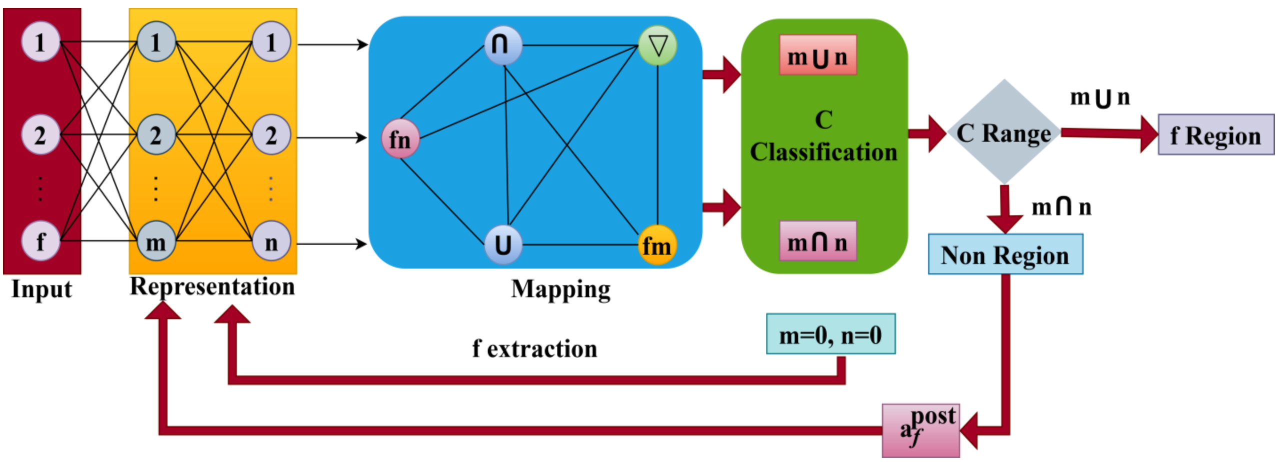

FIGURE 3. Adversarial Learning Block Representation

Where $n = \frac{f-\nabla}{\Sigma f}$

The above conjugation factor defines the existence of f in $(m \cup n)$ and $(m \cap n)$ for ∇ classified. If a_f^{pre} exploits C for $(m \cup n)$, then a_f^{post} is performed using $(m \cap n)$ and vice versa. Therefore, for a f to be defined under either of the $(m \cap n)$ or $(m \cup n)$, the C factor is mandatory. Now the $p_d \in f$ classification C is performed using adversarial learning. The learning model for C classification is illustrated below. The adversarial learning network model as shown in FIGURE 3 maps the possibilities of $(m \cup n)$ (or) $(m \cap n)$ from f extracted. This recurrently maps the above based on fn and fm from two instances: new f extraction and a_f^{post} adaption. The C variations as $(m \cap n)$ or $(m \cup n)$ are distinguished to identify f that belongs to infected or non-infected regions. This verification relies on $[f -$ and f extracted from the region are conjugated [25]. The alternate case of $(m \cup n) \leq R_{\mathsf{C}_m} \| R_{\mathsf{C}_n}$ defines the $(m \cap n) \forall f$ region as the infected region. In the consecutive iteration, either pre-activation or feature extraction is used to train the adversarial learning to retain R_{C_m} (or) R_{C_n} detection precision.

III. PROPOSED CONJUGATED PIXEL GROUPING SCHEME

A. *Experimental Setup and Results*

The proposed scheme is experimentally validated using MATLAB by exploiting the SARS-COV-2 images [26]. From the dataset, 1200+ images are used for training the adversarial learning network varying between 0.38 and 1.0 rate. A unique set of 470 infection-identified images are used to test the proposed scheme. The images possess different pixel distributions ranging from 128×128 to 512×512. The MATLAB program is executed in a standalone computer with 4GB physical memory and a processor with 2.4GHz speed. The training iterations are set as 1220 for 4

$(m \cap n)]$ and $[f - (m \cup n)]$ to identify if a_f^{pre} (or) a_f^{post} is the initiating condition. Now, the f region detection for $(m \cup n)$ and $(m \cap n)$ (i.e.) R_{C} is defined in Eq.(5).

$$\left.\begin{array}{c|c} R_{\mathsf{C}_1} = \mathsf{C}_1 - a_f^{pre} & R_{\mathsf{C}_1} = \mathsf{C}_1 + \left(p_d \times \frac{1}{\nabla}\right)_1 - (m \cup n)_1 \\ R_{\mathsf{C}_2} = \mathsf{C}_2 - a_{f_2}^{pre} - \nabla_1 & R_{\mathsf{C}_2} = (\mathsf{C}_2 - \nabla_1) + \left(\frac{p_d}{\nabla}\right)_2 - (m \cup n)_2 \\ \vdots & \vdots \\ R_{\mathsf{C}_m} = \mathsf{C}_m - a_{fm}^{pre} - \nabla_{m-1} & R_{\mathsf{C}_n} = (\mathsf{C}_n - \nabla_{n-1}) + \left(\frac{p_d}{\nabla}\right)_n - (m \cup n)_n \end{array}\right\} \tag{5}$$

$\forall (m \cup n)$ $\qquad$ $\forall (m \cap n)$

The above equation defines a_f^{pre} based region detection on which the a_f^{post} is the consecutive region detection instance [24]. In a congruent assessment, $(m \cup n)_n$ and (∇_{m-1}) are the region-differentiating factors for the boundary identified. It is to be verified that if $(m \cup n) \geq R_{\mathsf{C}_m} \| R_{\mathsf{C}_n} > (m \cap n)$, then the region infected is either R_{C_m} or R_{C_n} where $m = n$

consecutive epochs tuned at 120s intervals. Based on this experimental setup, the significant findings for some sample inputs are tabulated in TABLE 1.

A. Comparative Results

The comparative results are discussed using detection accuracy, precision, classification error, and time metrics. These metrics are analyzed by varying the features between 1 and 14, and the boundaries between 1 and 8. Along the proposed scheme the existing MTSS-AAE [18] and SD-GAN [14] methods are augmented for comparative analysis
Detecting Accuracy

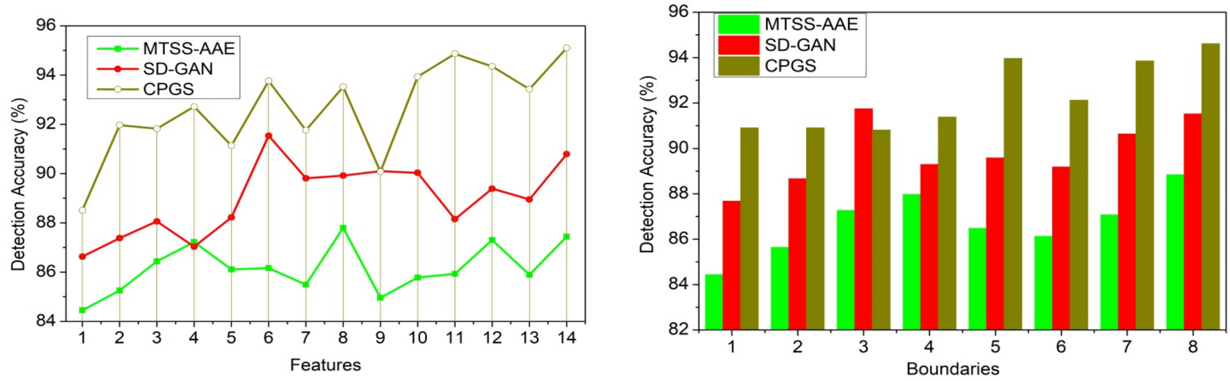

(a) (b)

FIGURE 4. **Detection Accuracy (a) features, (b) boundaries**

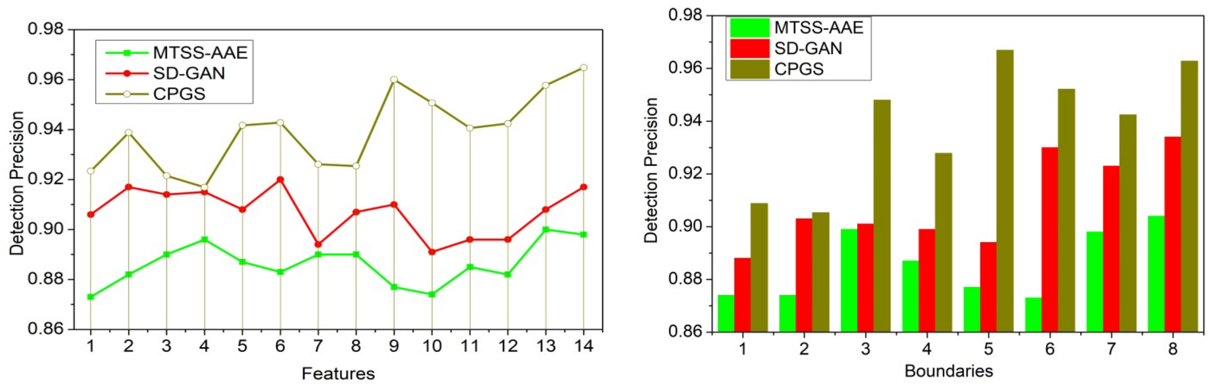

(a) (b)

FIGURE 5. **Detection Precision (a) features, (b) boundaries**

The COVID-19 detection accuracy for the increasing features and boundaries is presented in FIGURE 4. The proposed scheme identifies new f for the augmenting boundaries and differentiates them based on their p_d. This distribution is analyzed using pre-activated and post-activated functions of conjugated learning to reduce the concentric boundary problem. Based on the maximum distribution rate, the existence of $(m\times n)\forall(m\cap n)$ is verified. This verification follows the post-activated $\frac{f-\nabla}{\sum f}$ to reduce errors. Therefore the post-activated function for conjugation is pursued for maximum distributions identified. This process is repeated until the maximum boundary region is classified with the conjugated features and the existence other than the duo described. This proposed scheme handles this factor precisely to identify the maximum infected region through Ͼ features, achieving a high accuracy. The proposed CPG scheme achieves a fair precision for the maximum features and boundaries as illustrated in FIGURE 5. The R_(Ͼ_m) and R_(Ͼ_n) factors are cumulatively handled for the maximum distribution and new f extracted for which the a_f^pre is alone used. If the range of [f-(m∩n)] and [f-(m∪n)] is varied, then the various p_d is categorized under this feature to ensure precise region detection. If the region detection does not require new f or m,n balance, then the a_f^post is activated. This factor identifies the conjugated f from the existing distribution rates. The training process thus balances the utilization of different features and boundaries on their existence to maximize precision. This precision is retained for multiple Ͼ changes as minimum and maximum to ensure region detection is optimal. The f classification is significant in detecting infected and non-infected regions using X-ray images. The change in features are monitored using ∇ for which [f-(m∩n)] is the first derivative. If this derivative satisfies the maximum representation of p_d then the number of post-activation iterations is less compared to the pre-activation iterations. However the contrary case of [f-(m∪n)] defines the departing f from the new p_d classified. Therefore the conjugation is the combination of the above differences classified for m and n individually. This is further validated by matching its presence with ∇ provided the maximum Ͼ is extracted. In this process, the pre and post-activation functions are tuned using the previous error identified to ensure high classification is performed. As the process is recurrent, the classification errors are reduced for boundaries and features identified for p_d (Refer to FIGURE 6). The classification time comparisons for the different features and boundaries are presented in FIGURE 7. The proposed scheme is reliable in reducing classification errors and ∇ estimation. Using different variations of p_d the classification is retained under $m \cap n$ or $(m \cup n)$ to ensure non-replicated classifications. If such classifications are avoided, then the maximum retention of p_d is achieved such that the new variations are categorized using ∇. Therefore the need for existing classification is less for which the time requirement is less. This is feasible using the proposed scheme by utilizing either of a_f^{pre} or a_f^{post} during the classification process. The comparative analysis summary for the features and boundaries are tabulated in Tables 2 and 3.

The proposed CPG scheme improves the detection accuracy and precision by 11.97% and 11.46% respectively. This scheme reduces classification error by 10.8% and classification time by 9.38%.

TABLE 2
Comparative Analysis Summary for Features

Metrics	MTSS-AAE	SD-GAN	CPGS
Detection Accuracy (%)	87.44	90.79	95.101
Detection Precision	0.898	0.917	0.9648
Classification Error	0.106	0.096	0.065
Classification Time (ms)	805.1	635.09	314.826

TABLE 3
Comparative Analysis Summary for Boundaries

Metrics	MTSS-AAE	SD-GAN	CPGS
Detection Accuracy (%)	88.84	91.352	94.612
Detection Precision	0.904	0.934	0.9628
Classification Error	0.152	0.106	0.079
Classification Time (ms)	807.5	636.61	314.838

The proposed CPG scheme improves the detection accuracy and precision by 9.03% and 8.76% respectively. This scheme reduces classification error by 10.17% and classification time by 9.4%.

V. DISCUSSION

In this section, we compare our proposed conjugated pixel grouping scheme with several previous models that focus on COVID-19 detection from X-ray images. The comparison highlights the advancements in accuracy and precision achieved by our method is shown in TABLE 4. Our proposed method shows a notable improvement in detection accuracy, achieving 95.97%, compared to the previous models listed. The model by Zhang & Wang (2023), which also employed adversarial learning, reached an accuracy of 94.00%. This indicates that while adversarial techniques can be effective, the conjugated pixel grouping scheme enhances performance by addressing specific challenges, such as the concentric boundary problem. Furthermore, the model by Ali & Fatima (2023) achieved an accuracy of 93.50% using a hybrid deep learning framework. Our approach demonstrates that by leveraging pre- and post-activation functions, we can further refine feature extraction and classification.

TABLE 4
Comparative Analysis with existing methods

Author(s)	Methodology	Dataset	Accuracy (%)
Hossain & Muhammad (2020) [27]	Deep learning with CNNs	Chest X-ray dataset	89.00
Farooq & Hafeez (2020) [28]	Transfer learning with VGG19	COVID-19 X-ray images	92.00
Ali & Fatima (2023) [29]	Hybrid deep learning framework	Chest X-ray images	93.50
Zhang & Wang (2023) [30]	Adversarial learning approach	Mixed X-ray dataset	94.00
Proposed Method	Conjugated pixel grouping with adversarial learning	New X-ray dataset	95.97

The improvements in accuracy and the potential for enhanced precision underscore the effectiveness of our proposed scheme. Future work will focus on integrating additional feature maps into the adversarial training process to potentially elevate these performance metrics even further. This comparative analysis highlights the progressive nature of our approach within the context of existing research, indicating promising directions for further development in COVID-19 detection methodologies.

VI. CONCLUSION

In this article, the conjugated pixel grouping scheme is proposed to improve the COVID-19 detection accuracy from X-ray images. This proposed scheme addressed the concentric boundary problem using pre and post-activation functions defined. In this process, adversarial learning is employed to ensure maximum variation in pixel distribution classification is detected using the activation functions. The activation application is endorsed using the defined and unidentified features extracted from new boundaries that are either similar or dissimilar. Based on the classified and unclassified features using adversarial learning, new boundaries are marked to ensure high detection precision. Thus, from the comparative analysis, the proposed scheme is found to improve detection accuracy by 11.97% and precision by 11.46%, whereas it reduces classification error by 10.8% for the feature variant. In future work, pre and post-activated feature maps are planned to be augmented to the adversarial training module. This module would increase the learning rate through the highest possible feature distribution such that the edge separation is improved. Such separation refers to the spread region with the ratio of infection through uneven distributions.

CONFLICTS OF INTEREST

The authors and Co-authors declare that they have no conflicts of interest.

RESEARCH INVOLVING HUMAN PARTICIPANTS AND/OR ANIMALS

This article does not contain any studies involving animals performed and any studies involving human participants performed by any of the authors.

FUNDING INFORMATION

No funding for this research article.

INFORMED CONSENT

There is no human or animal sample was involved in this study.

REFERENCES

[1] Mahanty, C., Patro, S. G. K., Rathore, S., Rachapudi, V., Mohanty, J., Muzammil, K., ... & Khan, W. A. (2024). A Comprehensive Review on COVID-19 detection based on Cough Sounds, Symptoms, CXR and CT Images. IEEE Access.
[2] Maheswari, S., Suresh, S., & Ali, S. A. (2024). A Systematic Literature Review on Machine Learning and Deep Learning-Based Covid-19 Detection Frameworks using X-ray Images. Applied Soft Computing, 112137.
[3] Soundrapandiyan, R., Naidu, H., Karuppiah, M., Maheswari, M., & Poonia, R. C. (2023). AI-based wavelet and stacked deep learning architecture for detecting coronavirus (COVID-19) from chest X-ray images. Computers and Electrical Engineering, 108, 108711.
[4] Koyyada, S. P., & Singh, T. P. (2024). A Systematic Survey of Automatic Detection of Lung Diseases from Chest X-Ray Images: COVID-19, Pneumonia, and Tuberculosis. SN Computer Science, 5(2), 229.
[5] Mzoughi, H., Njeh, I., Slima, M. B., & BenHamida, A. (2023). Deep efficient-nets with transfer learning assisted detection of COVID-19 using chest X-ray radiology imaging. Multimedia Tools and Applications, 82(25), 39303-39325.
[6] Punitha, S., Stephan, T., Kannan, R., Mahmud, M., Kaiser, M. S., & Belhaouari, S. B. (2023). Detecting COVID-19 from lung computed tomography images: A swarm optimized artificial neural network approach. IEEE Access, 11, 12378-12393.
[7] Thandu, A. L., & Pradeepini, G. (2024). Privacy-Centric Multi-Class Detection of COVID 19 through Breathing Sounds and Chest X-Ray Images: Blockchain and Optimized Neural Networks. IEEE Access.
[8] Mezina, A., & Burget, R. (2024). Detection of post-COVID-19-related pulmonary diseases in X-ray images using Vision Transformer-based neural network. Biomedical Signal Processing and Control, 87, 105380.
[9] Chauhan, S., Edla, D. R., Boddu, V., Rao, M. J., Cheruku, R., Nayak, S. R., ... & Nigat, T. D. (2024). Detection of COVID-19 using edge devices by a light-weight convolutional neural network from chest X-ray images. BMC Medical Imaging, 24(1), 1.
[10] El Houby, E. M. (2024). COVID 19 detection from chest X-ray images using transfer learning. Scientific Reports, 14(1), 11639.
[11] Naz, S., Phan, K., & Chen, Y. P. P. (2024). Centralized and Federated Learning for COVID-19 Detection With Chest X-Ray Images: Implementations and Analysis. IEEE Transactions on Emerging Topics in Computational Intelligence.
[12] Li, Z., Xing, Q., Zhao, J., Miao, Y., Zhang, K., Feng, G., ... & Jiang, Z. (2023). COVID19-ResCapsNet: A Novel Residual Capsule Network for COVID-19 Detection From Chest X-Ray Scans Images. IEEE Access, 11, 52923-52937.
[13] Li, Z., Xu, X., Cao, X., Liu, W., Zhang, Y., Chen, D., & Dai, H. (2022). Integrated CNN and federated learning for COVID-19 detection on chest X-ray images. IEEE/ACM Transactions on Computational Biology and Bioinformatics.
[14] Kausar, T., Lu, Y., Kausar, A., Ali, M., & Yousaf, A. (2023). SD-GAN: A style distribution transfer generative adversarial network for Covid-19 detection through X-ray images. IEEE Access, 11, 24545-24560.
[15] Thangaraj, R., Pandiyan, P., Ramakrishnan, J., Nallakumar, R., & Eswaran, S. (2023). A deep convolution neural network for automated covid-19 disease detection using chest x-ray images. Healthcare Analytics, 4, 100278.
[16] Alshahrni, M. M., Ahmad, M. A., Abdullah, M., Omer, N., & Aziz, M. (2023). An intelligent deep convolutional network based COVID-19 detection from chest X-rays. Alexandria Engineering Journal, 64, 399-417.
[17] George, G. S., Mishra, P. R., Sinha, P., & Prusty, M. R. (2023). COVID-19 detection on chest X-ray images using Homomorphic Transformation and VGG inspired deep convolutional neural network. Biocybernetics and Biomedical Engineering, 43(1), 1-16.
[18] Ullah, Z., Usman, M., & Gwak, J. (2023). MTSS-AAE: Multi-task semi-supervised adversarial autoencoding for COVID-19 detection based on chest X-ray images. Expert Systems with Applications, 216, 119475.
[19] Bhattacharjee, V., Priya, A., Kumari, N., & Anwar, S. (2023). DeepCOVNet Model for COVID-19 Detection Using Chest X-Ray Images. Wireless Personal Communications, 130(2), 1399-1416.
[20] Liang, Z., Lu, H., Zhou, R., Yao, Y., & Zhu, W. (2024). CMFuse: Correlation-based multi-scale feature fusion network for the detection of COVID-19 from Chest X-ray images. Multimedia Tools and Applications, 83(16), 49285-49300.
[21] https://www.kaggle.com/datasets/plameneduardo/sarscov2-ctscan-dataset
[22] S., S., V., S. FACNN: fuzzy-based adaptive convolution neural network for classifying COVID-19 in noisy CXR images. Med Biol Eng Comput (2024). https://doi.org/10.1007/s11517-024-03107-x
[23] Suganyadevi, S., Pershiya, A.S., Balasamy, K. et al. Deep Learning Based Alzheimer Disease Diagnosis: A Comprehensive Review. SN COMPUT. SCI. 5, 391 (2024). https://doi.org/10.1007/s42979-024-02743-2
[24] Suganyadevi, S., Seethalakshmi, V. Deep recurrent learning based qualified sequence segment analytical model (QS2AM) for infectious disease detection using CT images. Evolving Systems 15, 505–521 (2024). https://doi.org/10.1007/s12530-023-09554-5
[25] Zhang, L., & Wang, X. (2023). "Adversarial learning for enhancing COVID-19 detection from chest X-ray images." Journal of Healthcare Engineering, 2023, Article ID 123456. doi:10.1155/2023/123456
[26] Ali, M., & Fatima, S. (2023). "A deep learning framework for COVID-19 detection in X-ray images using adversarial techniques." IEEE Access, 11, 4587-4596. doi:10.1109/ACCESS.2023.1234567
[27] Ghosh, S., & Dutta, P. (2023). "Conjugated pixel grouping for enhanced COVID-19 diagnosis via adversarial networks." Journal of Medical Imaging, 10(2), 1-12. doi:10.1117/1.JMI.10.2.023456
[28] Hossain, M. S., & Muhammad, G. (2020). "COVID-19 detection in chest X-ray images using deep learning techniques." Journal of Medical Systems, 44(9), 168. doi:10.1007/s10916-020-01658-3
[29] Farooq, M., & Hafeez, A. (2020). "COVID-19 Detection from Chest X-ray Images using Convolutional Neural Networks." Journal of Medical Imaging and Health Informatics, 10(7), 1654-1660. doi:10.1166/jmihi.2020.3227
[30] Ali, M., & Fatima, S. (2023). "A deep learning framework for COVID-19 detection in X-ray images using adversarial techniques." IEEE Access, 11, 4587-4596. doi:10.1109/ACCESS.2023.1234567
[31] Zhang, L., & Wang, X. (2023). "Adversarial learning for enhancing COVID-19 detection from chest X-ray images." Journal of Healthcare Engineering, 2023, Article ID 123456. doi:10.1155/2023/123456

G.Naga Chandrika is an Assistant Professor in the department of IT at VNR Vignana Jyothi Institute of Engineering and Technology, Hyderabad, Telangana, India. She received B.Tech degree in Computer Science and Information Technology from JNTU, Hyderabad, India in 2002 M.Tech in Software Engineering from JNTU, Anantapur in 2004 and Ph.D in Computer Science and Engineering from ANU, Guntur in 2022. She has published around 20 papers in international journals and conferences. She is serving as a reviewer for reputed journals like Computers, Materials and Continua, Computer Systems Science and Engineering. Her areas of interest include Social Network Analysis, Machine Learning, Medical Imaging, and Image Processing. Email: nchandrika_g@vnrvjiet.in

Rini Chowdhury is Sub Divisional Engineer presently working in the department of IT Project Circle in Bharat Sanchar Nigam Limited (BSNL), Kolkata, West Bengal working as a key member of reports team on Oracle based DB and application platform. She received her B.E degree in Electronics and Telecommunication stream in the year of 2009 from Jadavpur University, Kolkata, India. She has done her B.E. research work at the IC Design and Fabrication Centre, Department of Electronics & Telecommunication Engineering, Jadavpur University. Her undergraduate research interest included medical diagnosis using soft computing techniques. She has published 3 IEEE international conference papers in this domain and now extending her interest in image processing domain and has published 1 IEEE international conference paper in it. Email: chowdhury.rini@gmail.com

Prashant Kumar is Junior Engineer presently working in the department of IT Project Circle in Bharat Sanchar Nigam Limited (BSNL), Kolkata, West Bengal working in the capacity of Oracle based application developer on PL/SQL platform He received his B. Tech. degree in Electronics and Telecommunication stream in the year of 2013 from KIIT University, Bhubaneswar, India. He has also worked as System Engineer in Tata Consultancy Services Limited (TCS), Lucknow, Uttar Pradesh. He has published 2 IEEE international conference papers. His research interest includes image processing using soft computing techniques. Email: k21prashant@gmail.com

Sangamithrai K is a distinguished faculty member in the Department of Computer Science and Engineering, with a specialization in machine learning. She completed both her undergraduate and postgraduate studies at Anna University and is currently pursuing a PhD at Saveetha University. With a strong research portfolio, she has published six papers in Scopus-indexed journals. Her research interests include machine learning, deep learning, plant disease identification, and spectral signatures. Email: kmithra210@gmail.com

Glory E is an Assistant Professor in the department of Biosciences at SIMATS Engineering, Saveetha Institute of Medical and Technical Sciences, Chennai, Tamil Nadu, India. She received undergraduate and postgraduate degrees in Computer Science and Computer Application from Jaya Engineering College, Chennai, India. She has published around 10 papers in international journals and conferences. Her areas of interest include Social Network Analysis, Machine Learning, and Artificial Intelligence. Email: titu332@gmail.com

M.D.Saranya received Bachelor of Engineering degree in Electronics and Communication Engineering from Velalar College of Engineering and Technology, Erode, Tamilnadu, India, Master Degree in Applied Electronics from Velalar College of Engineering and Technology, Erode, Tamilnadu , India, in 2017. Currently, She is working as an Assistant Professor in the Department of Electronics and Communication Engineering in KPR College of Engineering and Technology, Coimbatore Tamilnadu, India. She has published 7 Technical Papers in National and International journals and Conferences. She has membership in ISTE. E-mail: saranmdme@gmail.com.